U.S. DEPARTMENT OF ENERGY | Office of Science

NSTX-U

Divertor spectroscopy for radiative divertor feedback control and snowflake divertor experiments in NSTX Upgrade

V. A. Soukhanovskii, F. Scotti, M. E. Weller,

S. P. Gerhardt, R. Kaita, B. Stratton

Poster GP12.00091
57th Annual Meeting of the APS Division of Plasma Physics
Savannah, Georgia
November 16–20, 2015

Lawrence Livermore National Laboratory

PPPL

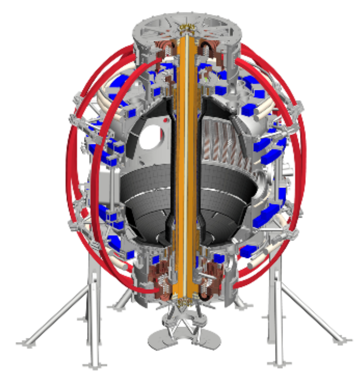

Abstract

In the NSTX-U tokamak, steady-state peak divertor heat fluxes are projected to reach 10-30 MW/m^2 thus challenging plasma facing component thermal limits. The snowflake divertor magnetic configuration and radiative divertor with feedback-controlled D_2 or impurity seeding are presently envisioned for divertor power handling, based on NSTX experiments and modeling with edge transport code UEDGE. In addition to the existing NSTX divertor diagnostics, new spectroscopic diagnostics are installed to improve understanding of snowflake divertor transport and to measure divertor radiation and plasma temperature for impurity radiation feedback control. A radially viewing divertor Phantom camera will be used to elucidate on the null-region churning mode. An upgraded vacuum ultraviolet spectrometer SPRED and a multichannel ultraviolet spectrometer would provide estimates of divertor impurity radiated power and divertor T_e~0.5-10 eV via the $\Delta n = 0; 1; 2$ of C and N line intensity ratios, and deuterium Balmer B7-B11 line ratios, respectively. The measurements are calibrated using atomic physics models and the collisional-radiative code CRETIN. Using the upgraded divertor gas injectors, the characteristic radiative divertor control time is expected to be under 50 ms.

Prepared under Contracts DE-AC52-07NA27344 and DE-AC02-09CH11466.

Outline

- Radiative divertor technique in standard and snowflake configurations are leading heat flux mitigation candidates in NSTX-U
- Radiative divertor control development (real-time T_e)
  - VUV spectrometer SPRED – carbon and nitrogen ion emission lines
  - UV-VIS spectrometer DIBS – deuterium Balmer lines and recombination continuum
- Snowflake divertor studies
  - Doppler spectroscopy, fast filterscopes and camera for churning mode, divertor turbulence and prompt particle loss studies

NSTX-U facility upgrades enable access to new parameter space and unique capabilities

Upgrades (NSTX → NSTX-U)	Operations year available	Boundary Physics area
P_{NBI} = 5 → 12 MW (5 s) 7.5 →15 MW (1.5 s)	1-2	Pedestal structure and ELM stability, L-H, divertor heat flux (12 → 15-20 MW/m^2) P/R ~ 10 → 20 P/S ~ 0.2 → 0.4
I_p = 1.3 → 2 MA B_t = 0.5 → 1 T	2-3	L-H transition, pedestal structure and stability, SOL width, divertor heat flux
Pulse length 1.5 → 5-10 s	1-3	Steady-state divertor heat flux mitigation, density and impurity control
Axisymmetric PF (divertor) coils PF1A, 1B, 1C, 2L	1-3	Plasma shaping, L-H, divertor configuration control
Non-axisymmetric control coils	3	ELM control and pedestal transport
Divertor cryogenic panel	3	Pedestal stability, density control, radiative divertor with impurity seeding
Molybdenum plasma-facing components	2	Core and pedestal impurity density, divertor heat transport regimes

Open geometry divertor with graphite PFCs will be used in initial years in NSTX-U

- Open divertor geometry
  - Low neutral and impurity compression
- No active divertor pumping
  - Lithium coatings for reduced recycling
  - Planned cryopump in future years
- Graphite plasma facing components
  - ATJ, POKO graphite and CFC tiles
    - Physical and chemical erosion
    - Dust
  - Max P_{rad} fraction limited by carbon radiation efficiency
- Four up-down symmetric divertor coils
  - Flexibility in divertor configurations
- Diagnostics: IR cameras, MPTS, Langmuir probes, filtered visible cameras, VUV-UV-VIS-NIR spectroscopy
  - Divertor Thomson scattering (incremental)

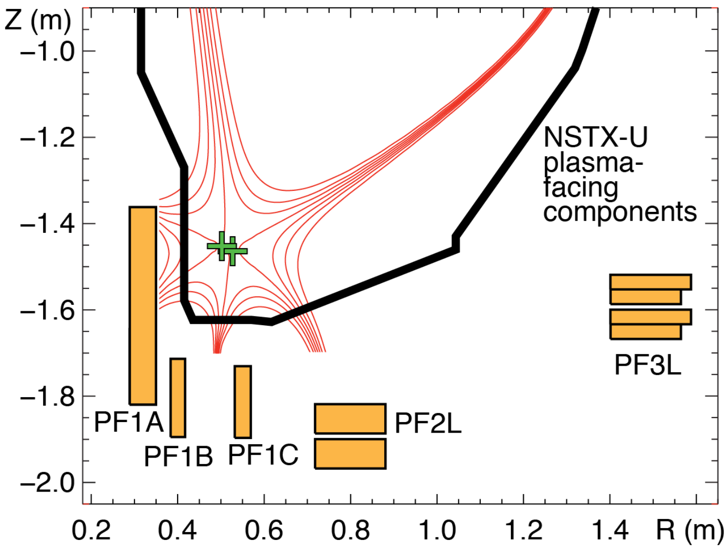

Radiative divertor technique in standard and snowflake configurations are leading heat flux mitigation candidates

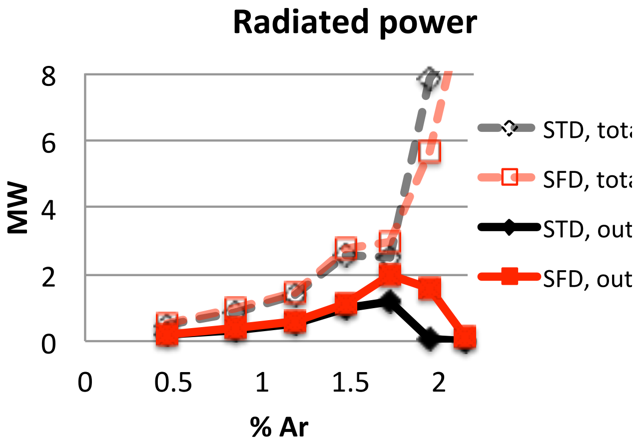

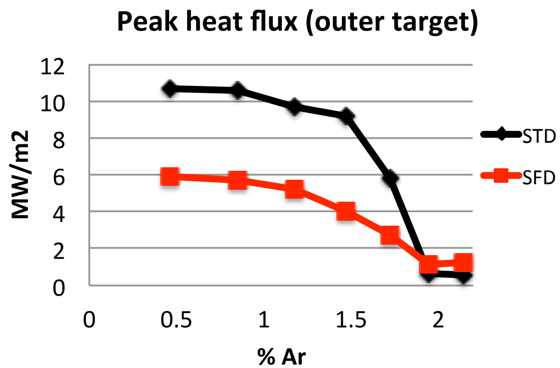

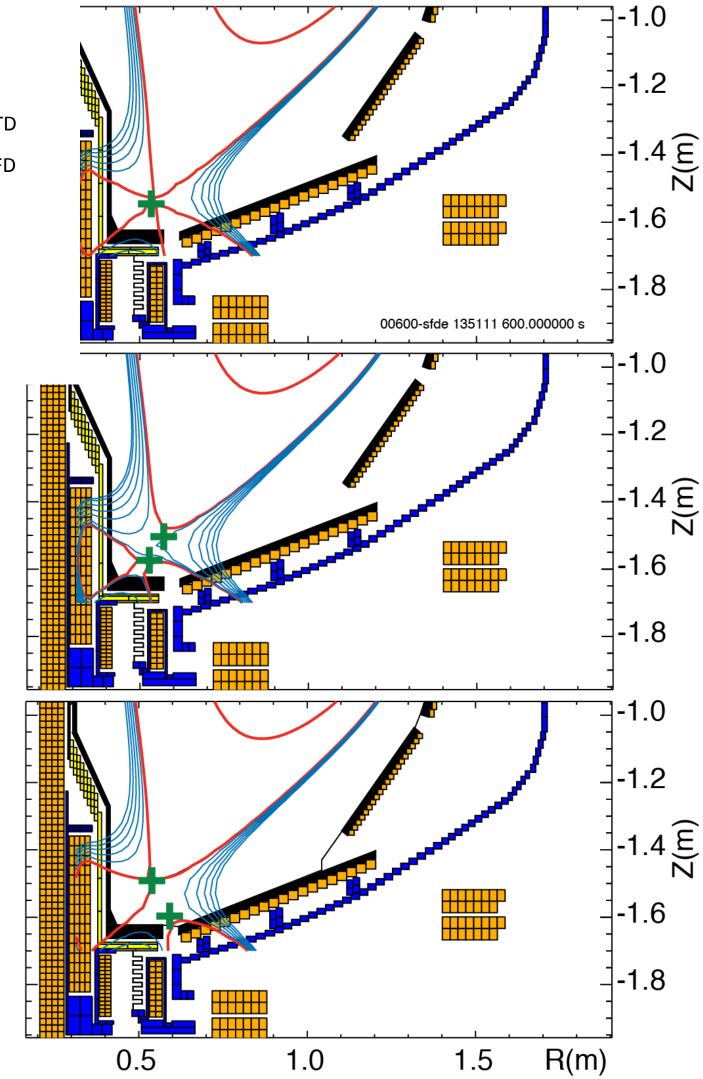

$$q_{pk} \simeq \frac{P_{heat}\,(1-f_{rad}) f_{out/tot} f_{down/tot} (1-f_{pfr}) \sin\alpha}{2\pi R_{SP} f_{exp} \lambda_{q_{||}}}$$

- Seeded impurity choice dictated by Z_{imp} and PFC
  - Li/C PFCs compatible with D_2, CD_4, Ne, Ar seeding
  - UEDGE simulations (E. T. Meier)
    - Ar most effective
    - Radiative collapse of pedestal if too much argon

Edge modeling predicts significant heat flux reduction with radiative snowflake divertor

- Snowflake with 3% carbon
- Wide density operational window as low as $n_e/n_G \leq 0.4$
  - Peak heat flux reduced up to 50% stronger (cf. standard radiative divertor) at lower n_e
  - Less impurity seeding (argon or neon) needed for lower peak heat flux
- Multi-fluid code UEDGE
  - B_t = 1.0 T, I_p = 2 MA, P_{SOL} = 9 MW
  - NSTX-like transport $\chi_{i,e}$=2-4 m^2/s, D=0.5 m^2/s

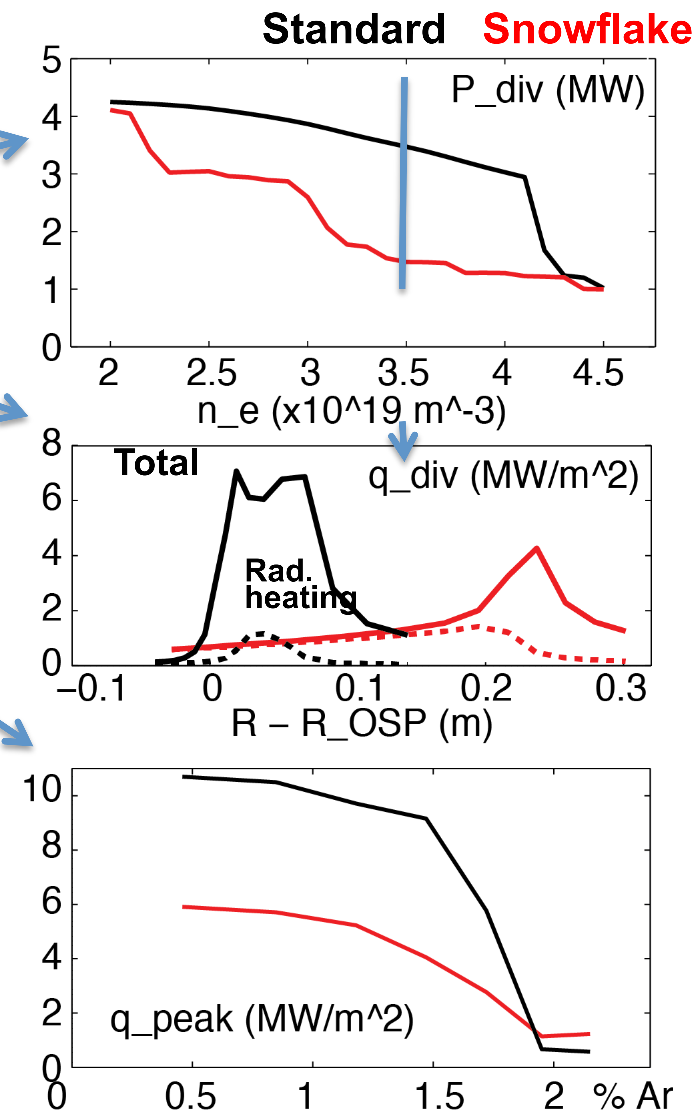

E. T. Meier et. al, Nucl. Fusion (2015)

Impurity-seeded radiative divertor with feedback control is planned for long discharges

- In NSTX, heat flux reduction in radiative divertor compatible with H-mode confinement was demonstrated with D_2 or CD_4 puffing
- Feedback control of divertor radiation via impurity particle balance control
  - Cryopump for particle removal
  - Divertor gas injectors
  - Real-time control signal diagnostics could include
    - PFC temperature via IR thermography or thermocouple
    - Thermoelectric current between inner and outer divertor
    - Impurity VUV spectroscopy or bolometry
    - Neutral gas pressure or electron-ion recombination rate
    - Spectroscopic T_e estimation

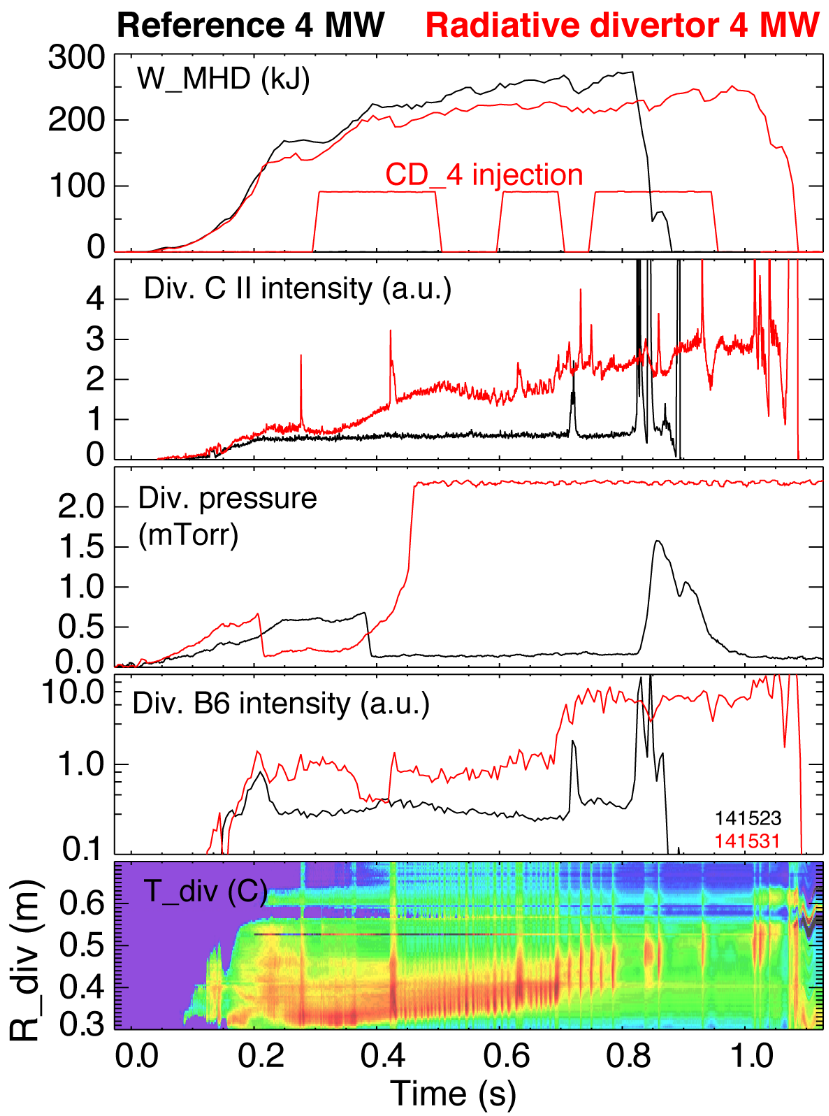

Conceptual design of radiative divertor feedback control system is based on PID control

- Proportional, integral, derivative controller

$$\Delta S = S_c - S_{ref}$$

$$V = K_0 + K_p \Delta S + K_i \int_{t_1}^{t_2} \Delta S dt + K_d \frac{d\Delta S}{dt}$$

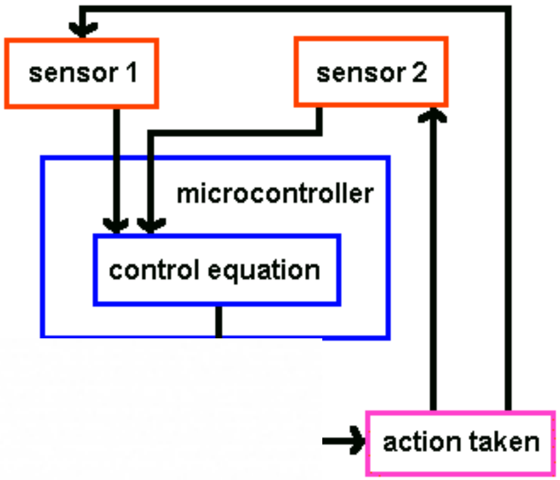

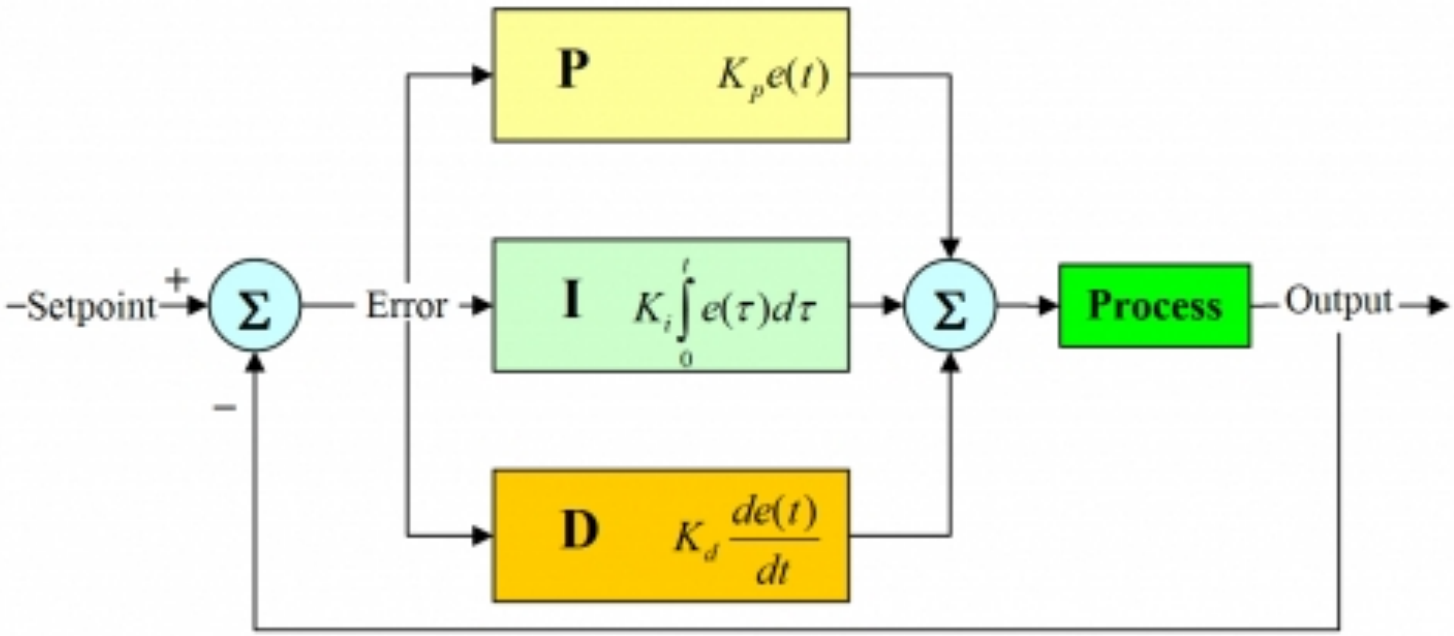

Control actuator – the new divertor gas injection system is being commissioned

- Four ½" OD SS divertor gas injection lines
- 2 upper and 2 lower
  - Copper backing plates modified to run tubing
  - Modification of 8 bullnose tiles
  - TIVs located at upper and lower outer vessel flanges

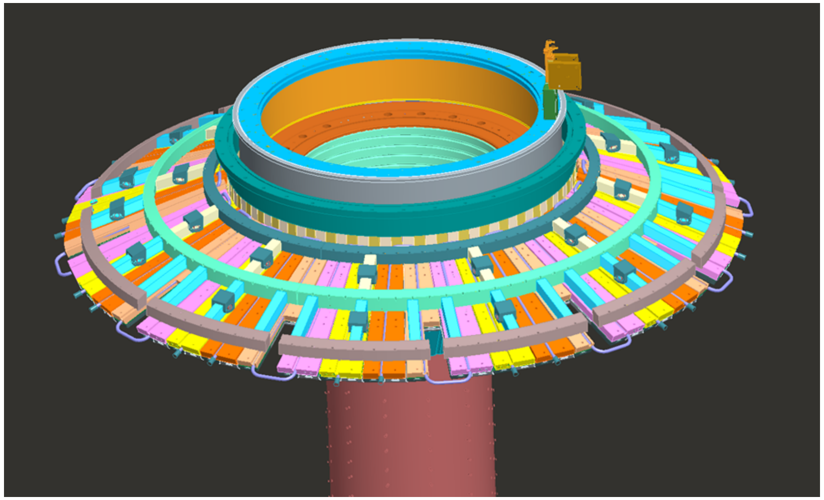

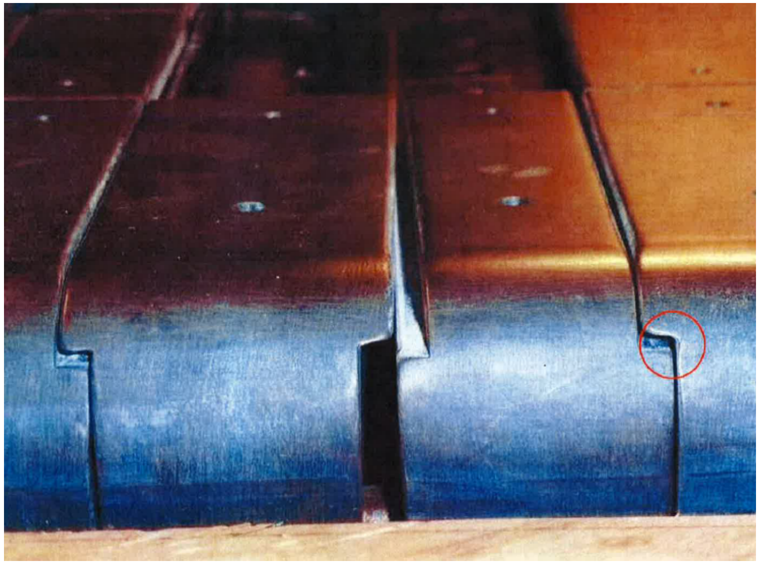

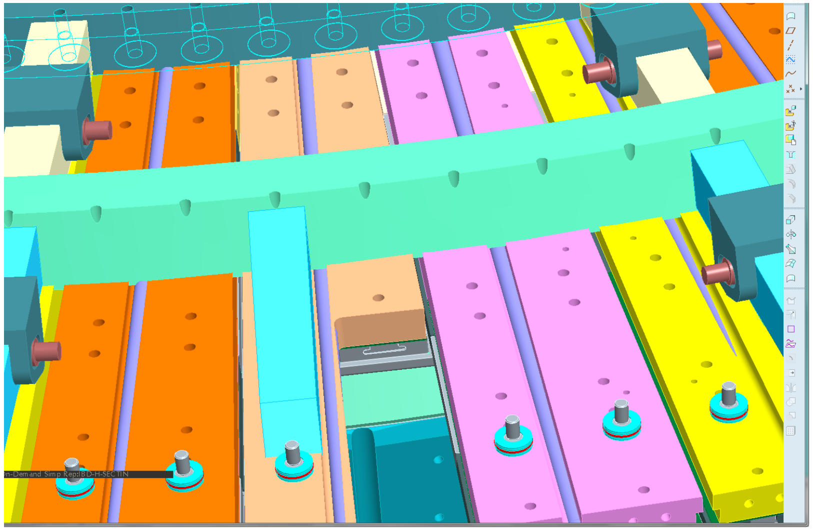

T_e-sensitive line intensity ratios are considered for divertor detachment control signal

- Balmer n=6-12 series lines in ion-neutral interaction zone $T_e \leq 5$ eV
  - Population kinetics is dominated by 3-body recombination at lower temperature
  - 3-body recombination rate

    $R \sim n_e^3\, T_e^{-4.5}$
  - Plasma is optically thin for Balmer lines
  - Dominated by Stark broadening due to linear Stark effect in electron and ion microfield. Other mechanisms neglected: Zeeman spitting, Van der Waals and natural broadening
  - Background due to bremsstrahlung and radiative recombination

$$\epsilon = 1.89 \times 10^{-28} \frac{n_e^2\, g_{ff}\, Z_{eff}}{\lambda^2 \sqrt{T_e}}\, e^{-\frac{12400}{T_e\, \lambda}}$$

$$I_{Z,z-1,n} = I_H \frac{z^2}{n^2} \qquad \frac{I_{Z,z-1,n}}{kT} \leq \frac{hc}{\lambda kT}$$

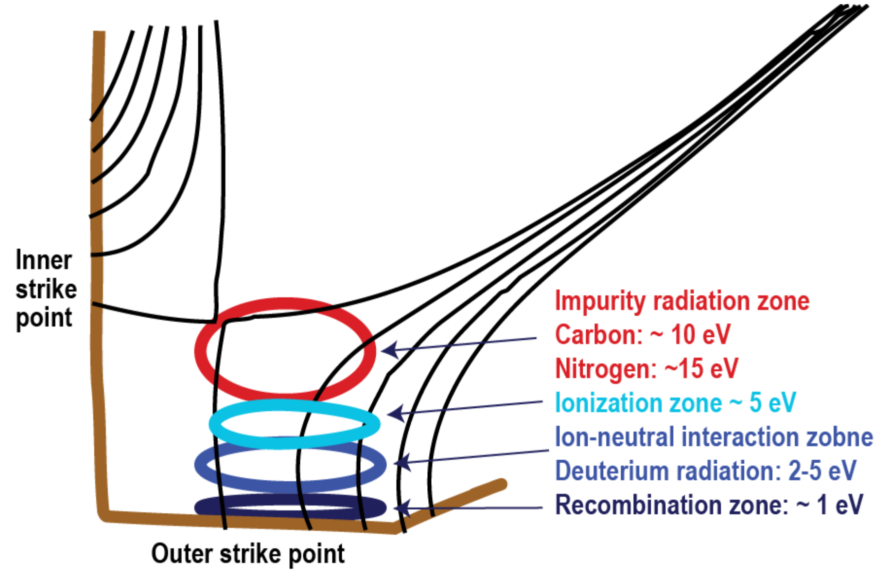

Figure concept after M. E. Fenstermacher, PPCF 1999

- Carbon or nitrogen Δn=0; 1; 2 lines in impurity radiation zone $T_e \leq 10$-15 eV
  - Intensity ratios highly T_e sensitive due to T_e sensitivity of excitation rates
  - Emission also proportional to impurity density

$$\frac{dP(\lambda,T)}{d\lambda} = \frac{2.051\times10^{-19}\, g_{ff}(z,\lambda,T)}{\lambda^2\, \sqrt{T_e}}\, \frac{I_H}{kT} N_e\, e^{\frac{hc}{\lambda kT}} \sum_{Z,z,n} g_{fb} \frac{\eta_{Z,z,n}}{n} \left(\frac{I_{Z,z-1,n}}{kT}\right)^2 \frac{N(Z^{+z})}{N(Z)} \frac{N(Z)}{N(H)} N(H)\, e^{\frac{I_{Z,z-1,n}}{kT}}$$

High-n Balmer line spectra used in NSTX for divertor recombination rate, T_e and n_e studies

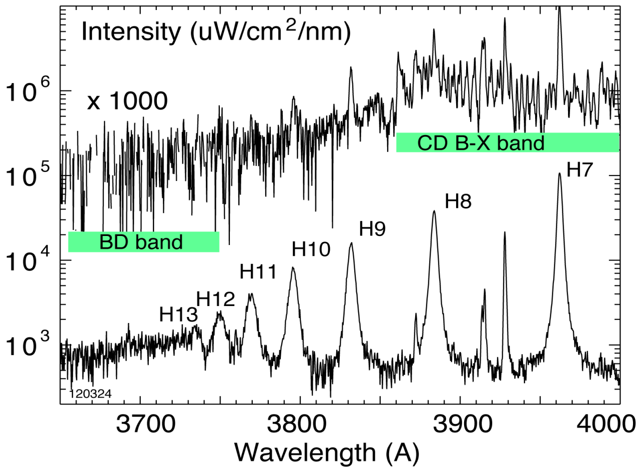

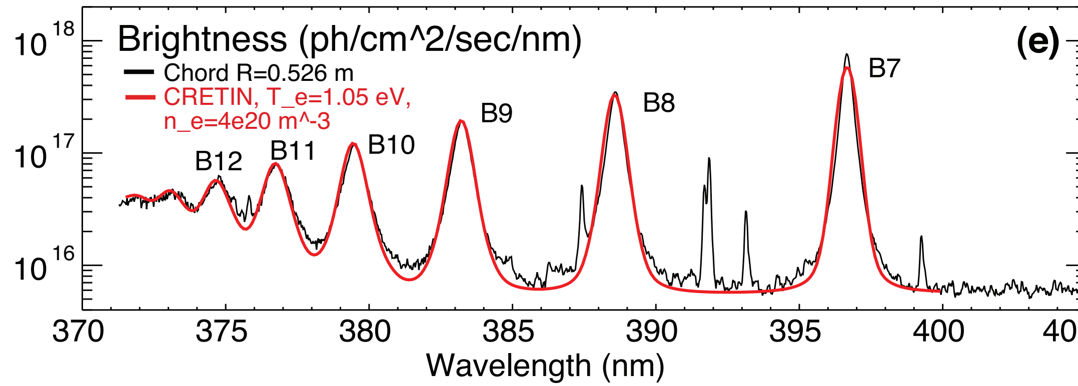

Free–bound continuum emission

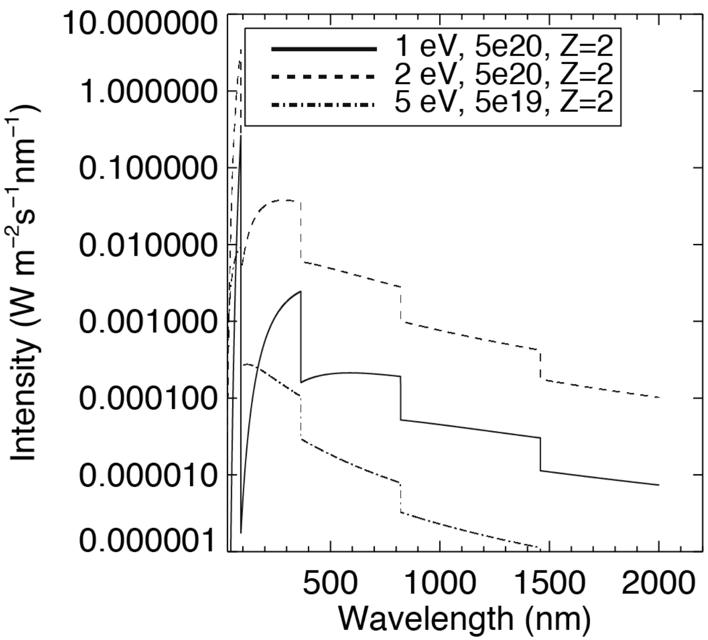

- Balmer series spectra modeled with CRETIN
- T_e=0.8-1.2 eV, n_e=2-7 x 10^{20} m^{-3} inferred from modeling
- Free-bound continuum modeled with CHIANTI

V. A. Soukhanovskii et al., Nucl. Fusion 2011
V. A. Soukhanovskii et al., RSI 2006

CRETIN code modeling used for T_e sensitivity of D, Li, C spectra

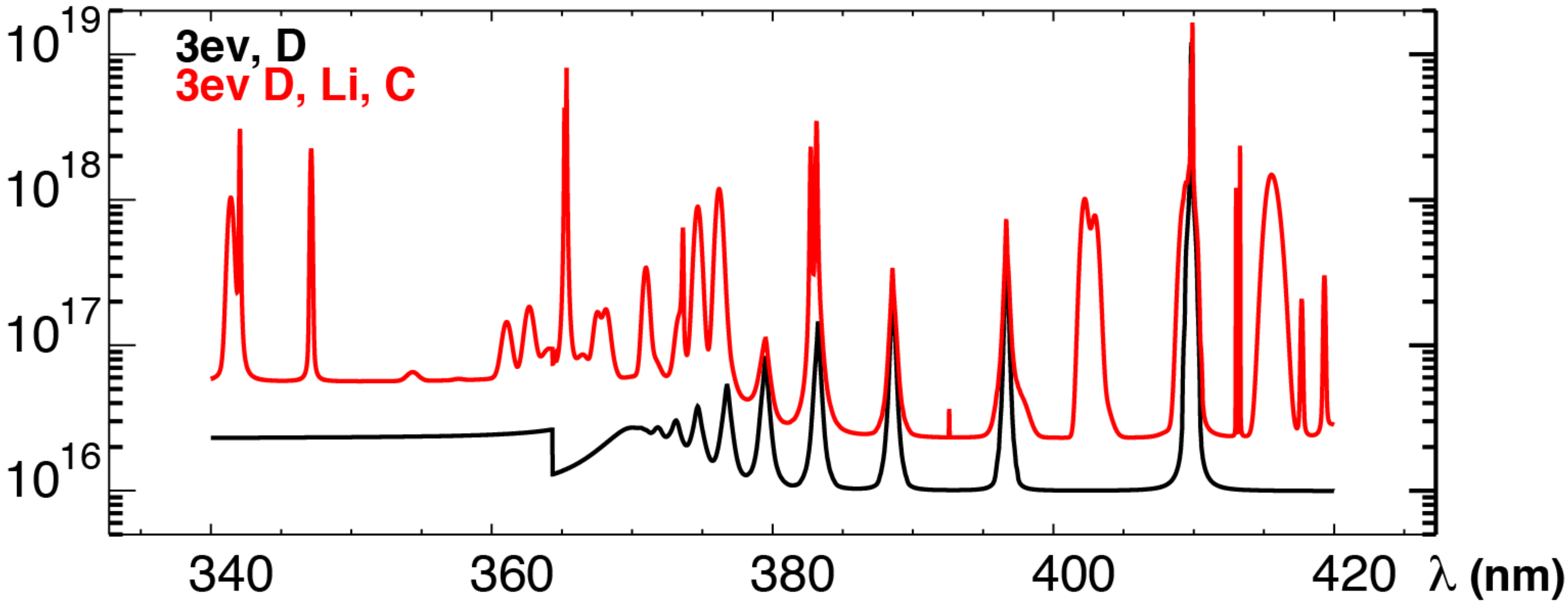

- CRETIN code is a collisional-radiative and radiation transport solver
  - H. Scott, J. Quant. Spectrosc. Radiat. Transf. 71 (2001) 689
  - Calculates whole spectrum including bremsstrahlung, line emission,line profiles, self-absorption, ionization and recombination
  - Includes NLTA population kinetics, radiation transport, neutral diffusion, diagnostic simulators
  - Line profiles code: TOTAL
    - Quasi-static approximation for ions, impact approximation for electrons
    - Electric dipole momentum reduced matrix elements must be calculated elsewhere
- Atomic data either from FAC or from hydrogenic model

T_e is estimated from Balmer line intensity ratio and from continua intensity ratio at Paschen jump

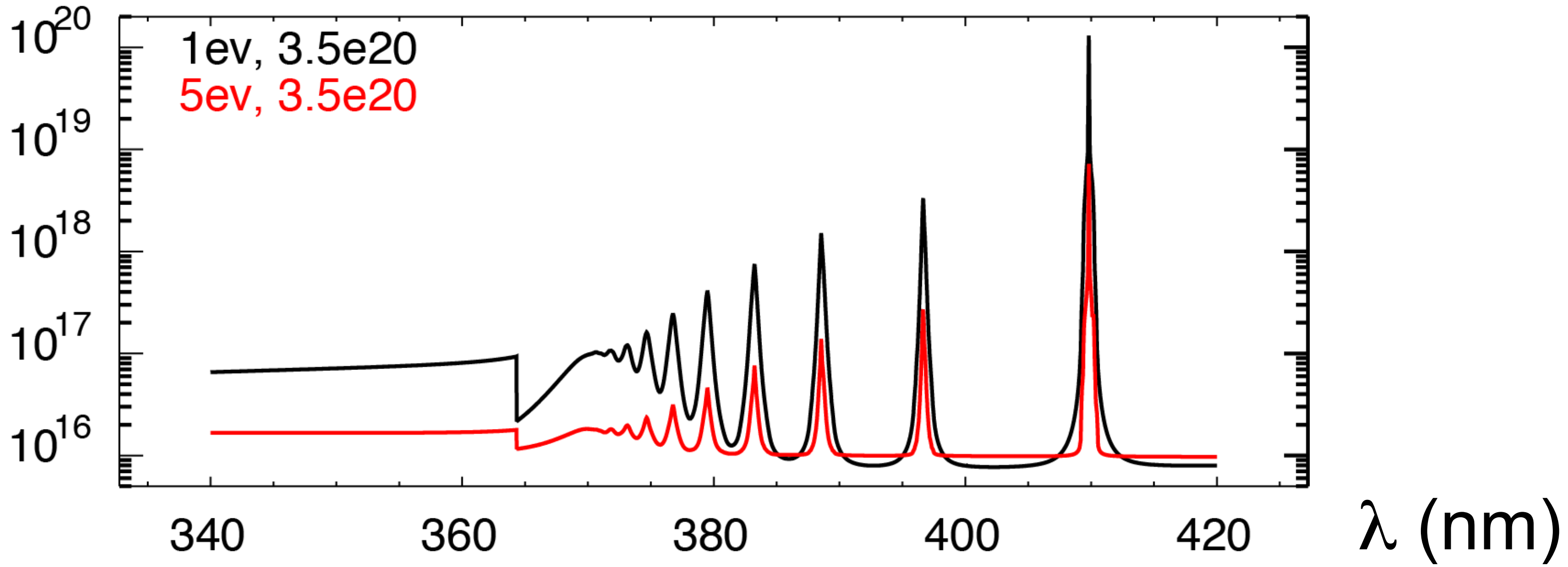

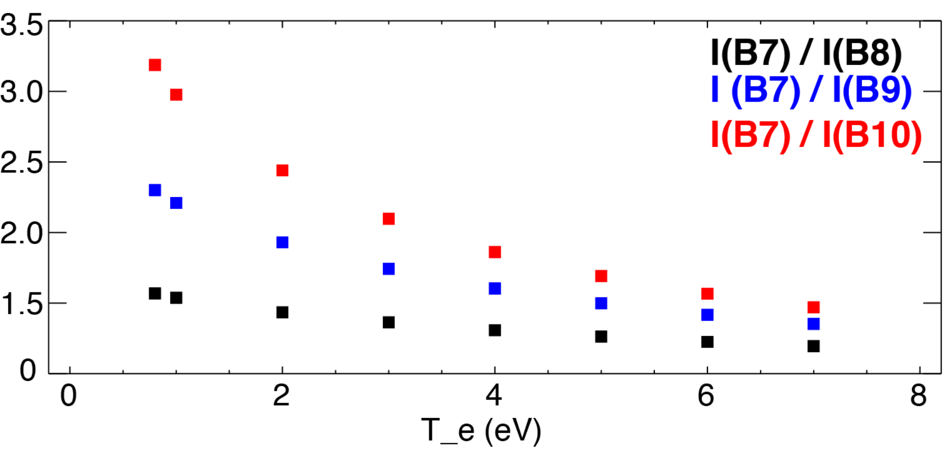

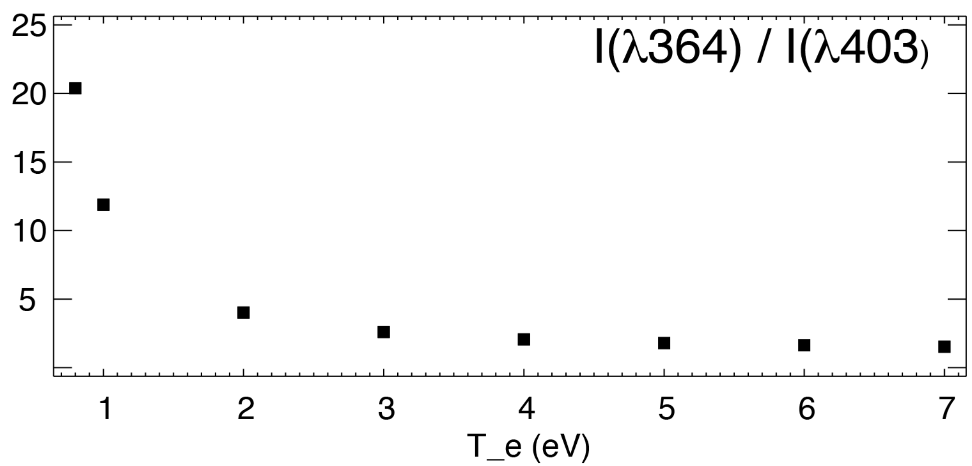

Carbon or nitrogen Li-like and Be-like ion Δn=0; 1; 2 line intensity ratios are T_e sensitive

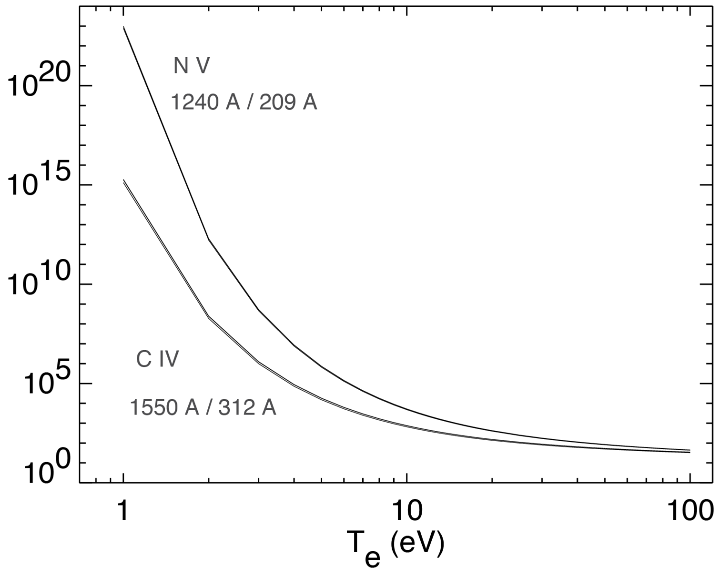

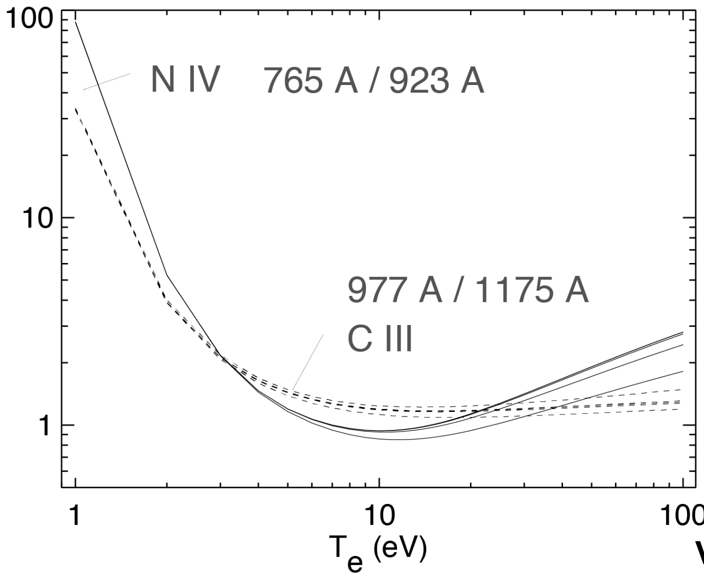

Table 1: Carbon and Nitrogen XUV/FUV lines due to $\Delta n = 0; 1; 2$ transitions.

Isosequence	Transition	Wavelength (Å) Carbon	Nitrogen
Li I-like	$2s\ ^2S_{1/2} - 2p\ ^2P_{3/2}$	1548.202	1238.821
	$2s\ ^2S_{1/2} - 2p\ ^2P_{1/2}$	1550.774	1242.804
	$2s\ ^2S_{1/2} - 3p\ ^2P_{1/2}$	312.418	209.274
	$2s\ ^2S_{1/2} - 3p\ ^2P_{3/2}$	312.455	209.308
	$2s\ ^2S_{1/2} - 4p\ ^2P_{3/2}$	244.907	162.556
	$2s\ ^2S_{1/2} - 4p\ ^2P_{1/2}$	...	162.564
Be I-like	$2s^2\ ^1S_0 - 2s2p\ ^3P_1$	1908.734	1486.496
	$2s^2\ ^1S_0 - 2s2p\ ^1P_1$	977.026	765.148
	$2s^2\ ^1S_0 - 2s3p\ ^1P_1$	386.203	247.205
	$2s^2\ ^1S_0 - 2s3p\ ^3P_1$	385.043	246.313
	$2s2p\ ^3P_2 - 2p^2\ ^3P_2$	1175.711	923.220
	$2s2p\ ^3P_1 - 2p^2\ ^3P_1$	1175.590	923.057
	$2s2p\ ^3P_2 - 2p^2\ ^3P_1$	1176.370	924.283
	$2s2p\ ^3P_1 - 2p^2\ ^3P_0$	1175.987	923.675
	$2s2p\ ^3P_1 - 2p^2\ ^3P_2$	1174.933	921.992
	$2s2p\ ^3P_0 - 2p^2\ ^3P_1$	1175.263	922.519
	$2s2p\ ^3P_2 - 2s3s\ ^3S_1$	538.312	322.722
	$2s2p\ ^3P_1 - 2s3s\ ^3S_1$	538.148	322.572
	$2s2p\ ^3P_0 - 2s3s\ ^3S_1$	538.080	322.506

V. A. Soukhanovskii, APS 1997

Carbon or nitrogen Li-like and Be-like ion Δn=0; 1; 2 line intensity ratios are T_e sensitive

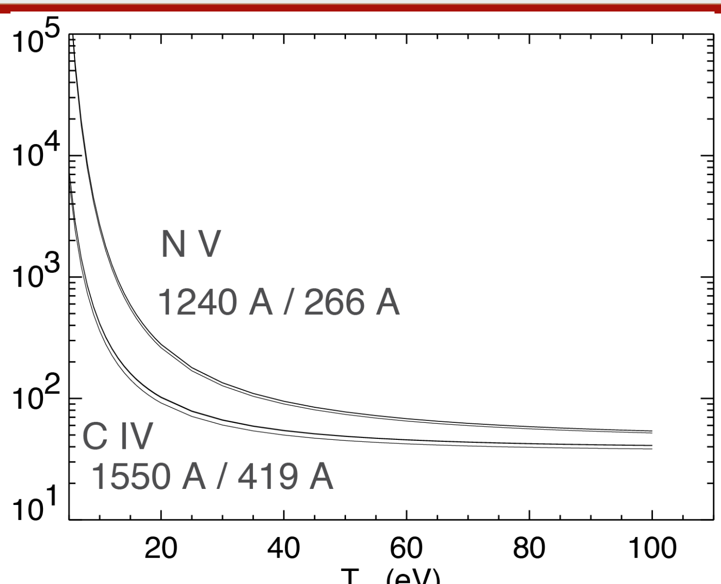

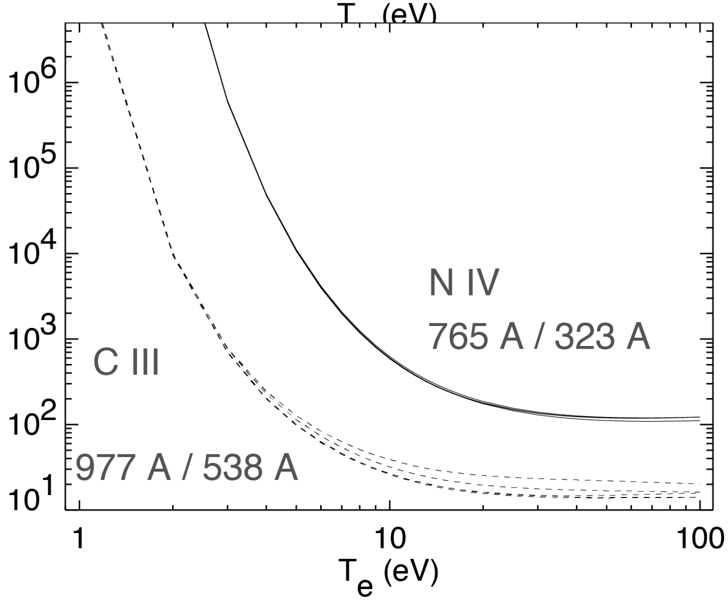

Table 1: Carbon and Nitrogen XUV/FUV lines due to $\Delta n = 0; 1; 2$ transitions.

Isosequence	Transition	Wavelength (Å) Carbon	Nitrogen
Li I-like	$2s\ ^2S_{1/2} - 2p\ ^2P_{3/2}$	1548.202	1238.821
	$2s\ ^2S_{1/2} - 2p\ ^2P_{1/2}$	1550.774	1242.804
	$2s\ ^2S_{1/2} - 3p\ ^2P_{1/2}$	312.418	209.274
	$2s\ ^2S_{1/2} - 3p\ ^2P_{3/2}$	312.455	209.308
	$2s\ ^2S_{1/2} - 4p\ ^2P_{3/2}$	244.907	162.556
	$2s\ ^2S_{1/2} - 4p\ ^2P_{1/2}$	...	162.564
Be I-like	$2s^2\ ^1S_0 - 2s2p\ ^3P_1$	1908.734	1486.496
	$2s^2\ ^1S_0 - 2s2p\ ^1P_1$	977.026	765.148
	$2s^2\ ^1S_0 - 2s3p\ ^1P_1$	386.203	247.205
	$2s^2\ ^1S_0 - 2s3p\ ^3P_1$	385.043	246.313
	$2s2p\ ^3P_2 - 2p^2\ ^3P_2$	1175.711	923.220
	$2s2p\ ^3P_1 - 2p^2\ ^3P_1$	1175.590	923.057
	$2s2p\ ^3P_2 - 2p^2\ ^3P_1$	1176.370	924.283
	$2s2p\ ^3P_1 - 2p^2\ ^3P_0$	1175.987	923.675
	$2s2p\ ^3P_1 - 2p^2\ ^3P_2$	1174.933	921.992
	$2s2p\ ^3P_0 - 2p^2\ ^3P_1$	1175.263	922.519
	$2s2p\ ^3P_2 - 2s3s\ ^3S_1$	538.312	322.722
	$2s2p\ ^3P_1 - 2s3s\ ^3S_1$	538.148	322.572
	$2s2p\ ^3P_0 - 2s3s\ ^3S_1$	538.080	322.506

V. A. Soukhanovskii, APS 1997

Cretin UV spectra simulations demonstrate feasibility of spectroscopic T_e measurements

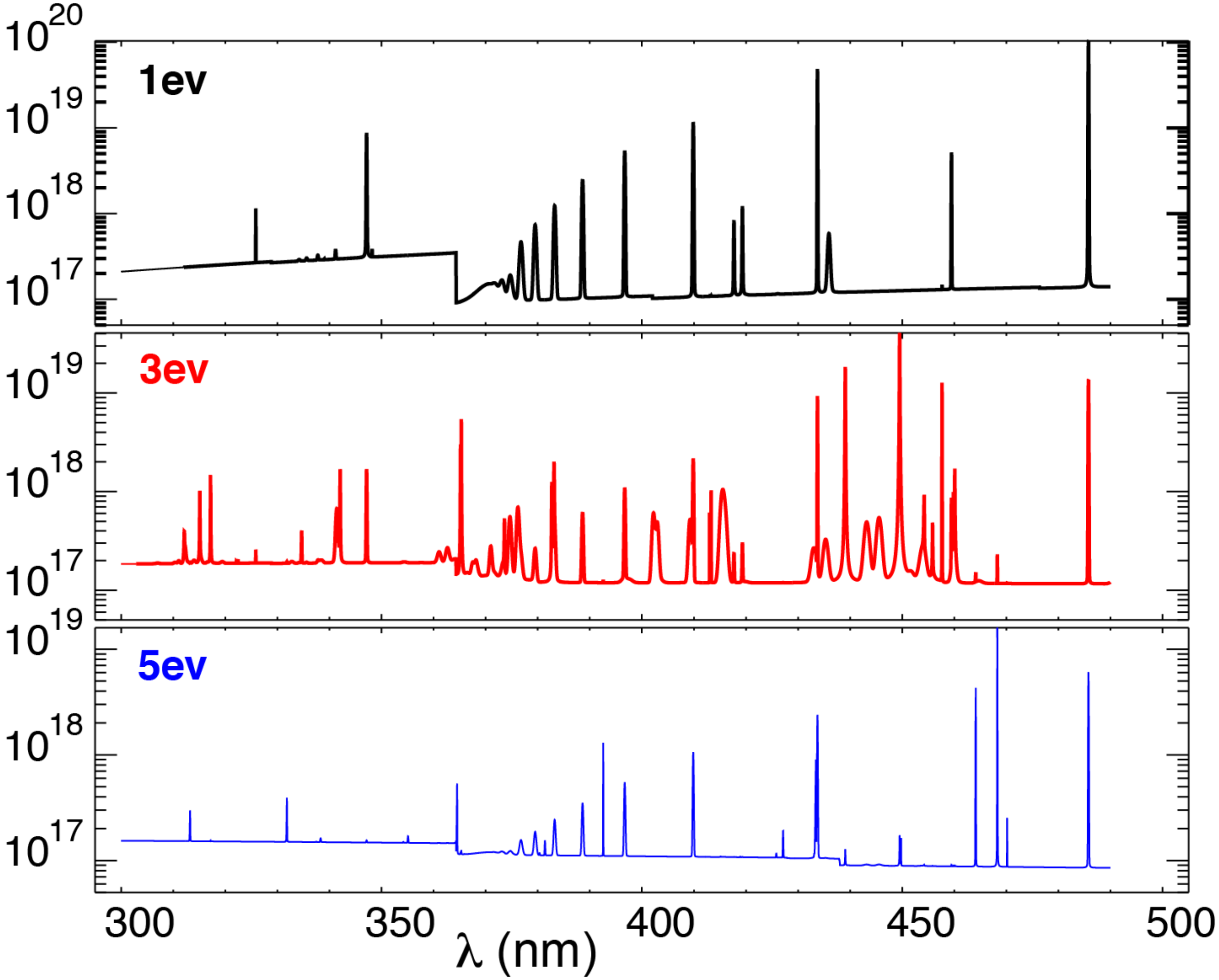

- S

Divertor imaging optics enables quasi-2D divertor emission measurements in UV-VIS-NIR

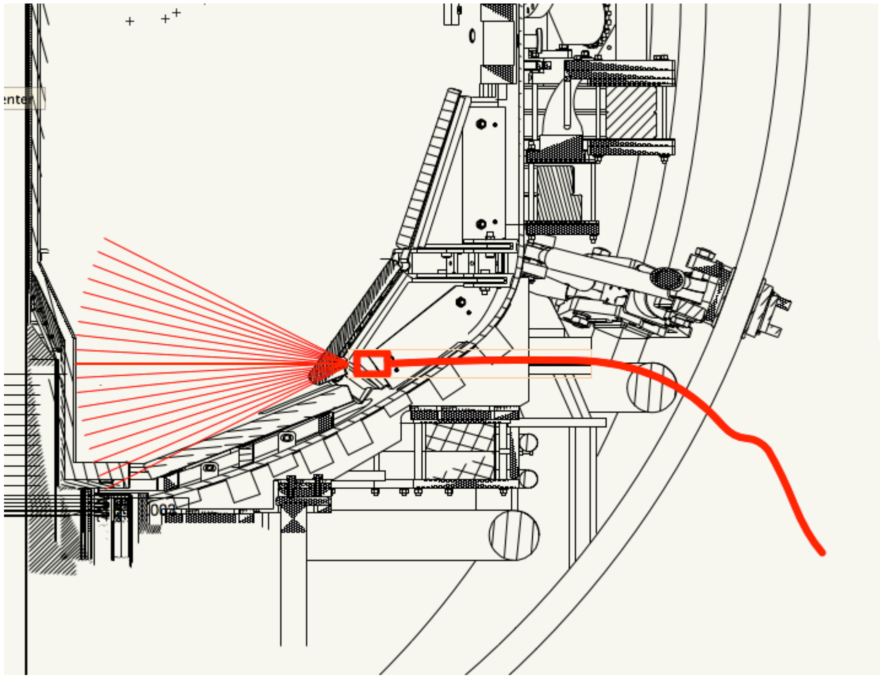

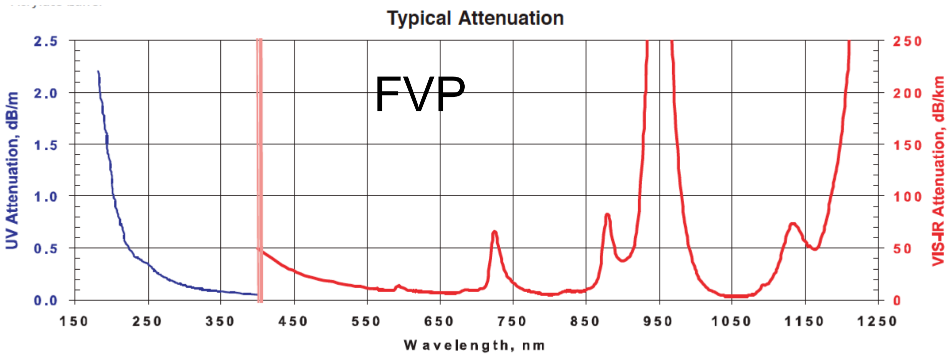

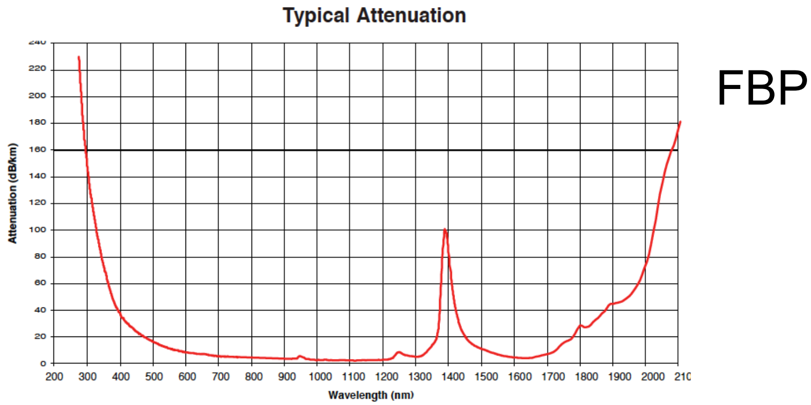

- 26-fiber bundle (Radiation resistant Molex FVP 200 um)
- 10-fiber bundle (Molex FBP 200 um)
- 30 m length
- Kogaku 8 or 12 mm imaging UV lens
- Fiber projection spot size 2-6 mm

Divertor Imaging Balmer Spectrometer (DIBS) enables fast line and continua measurements

- SCT 320 Czerny-Turner-Schmitt spectrograph
  - 600, 1200, 1800 gr/mm UV-VIS 68 mm gratings
- CCD camera PI ProEM 1600x400
- Real-time DAQ via WinSpec32 (pvcam)

PI IsoPlane SCT 320

Grating l/mm	CWL	Range (nm)	Short wl	Long wl	Dispersion nm/mm	CCD resolution (FWHM)	Bandwidth per pixel
600	399	124	336	461	4.849	0.14	0.078
1200	380 399	59 59	350 369	409 428	2.333 2.321	0.067 0.067	0.037 0.037
1800	399	37	380	417	1.452	0.044	0.023

Divertor SPRED spectrometer has broad applications for NSTX-U program

- Support plasma-facing component program
  - Steady-state and transient divertor impurity measurements
    - edge / divertor Mo III-XIV line emission
    - SOL / divertor Li II, Li III, C II, C III, C IV line emission
- Support divertor program
  - Divertor carbon ionization balance (steady-state and during ELMs)
  - Divertor T_e estimates from C II, C III, C IV line ratio (LR) measurements
    - Deviation from Maxwellian EEDF might be detected from these LR's
  - Improved divertor P_{rad} analysis
    - Most P_{rad} is due to several strong C III - C IV emission lines in the VUV
  - Radiative divertor impurity radiation (CD_4, N_2, Ne, Ar)
  - Detached divertor Lyman series for recombination rate, T_e, opacity

Divertor SPRED VUV spectrometer enables impurity emission measurement in outer divertor leg

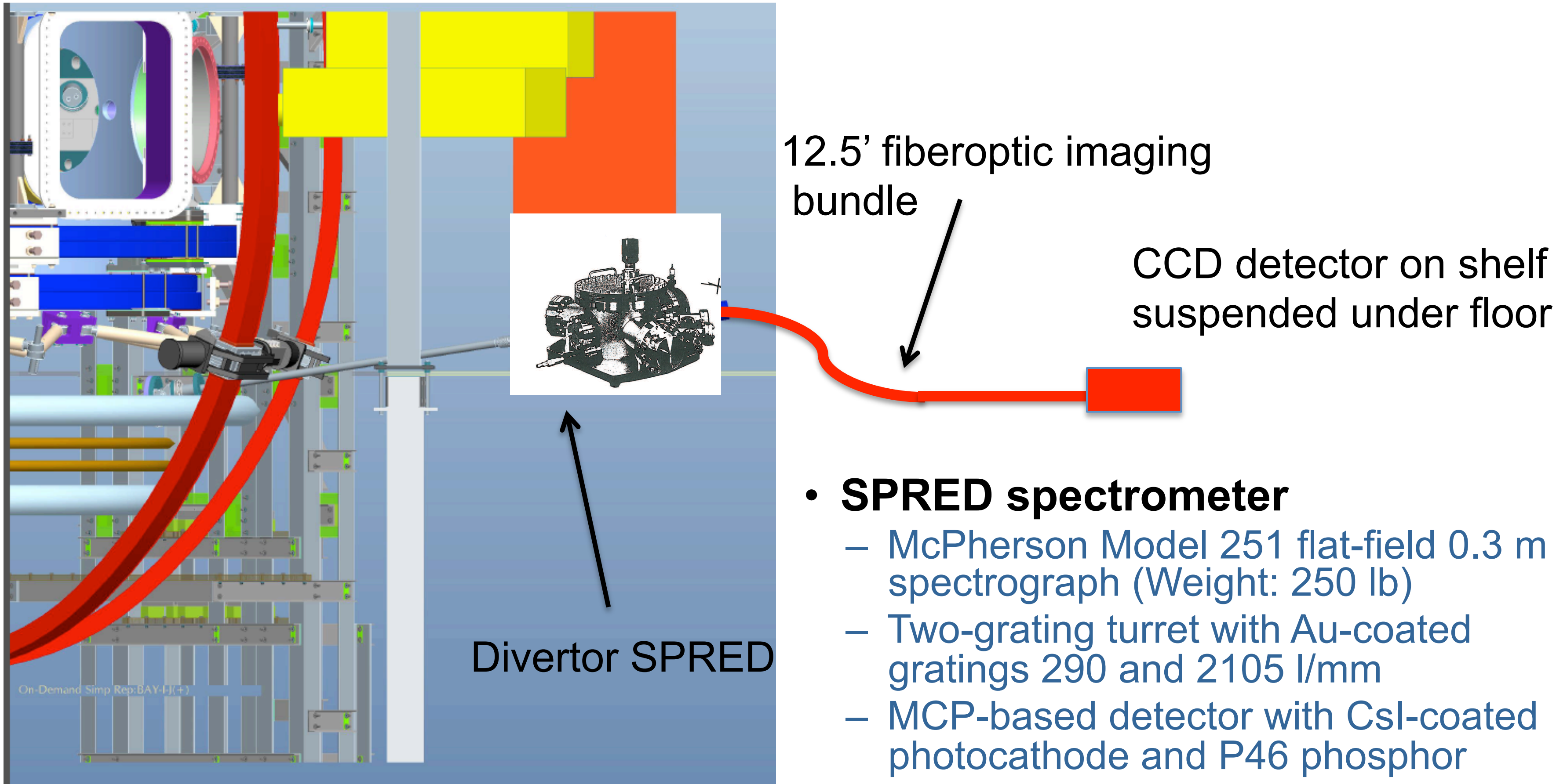

- **SPRED spectrometer**
  - McPherson Model 251 flat-field 0.3 m spectrograph (Weight: 250 lb)
  - Two-grating turret with Au-coated gratings 290 and 2105 l/mm
  - MCP-based detector with CsI-coated photocathode and P46 phosphor
  - Ion pump with controller
  - Schott 12 ft imaging bundle 25x4 mm
  - Princeton Instruments Pro-EM 1600x200 camera

Laboratory spectral measurements with divertor SPRED

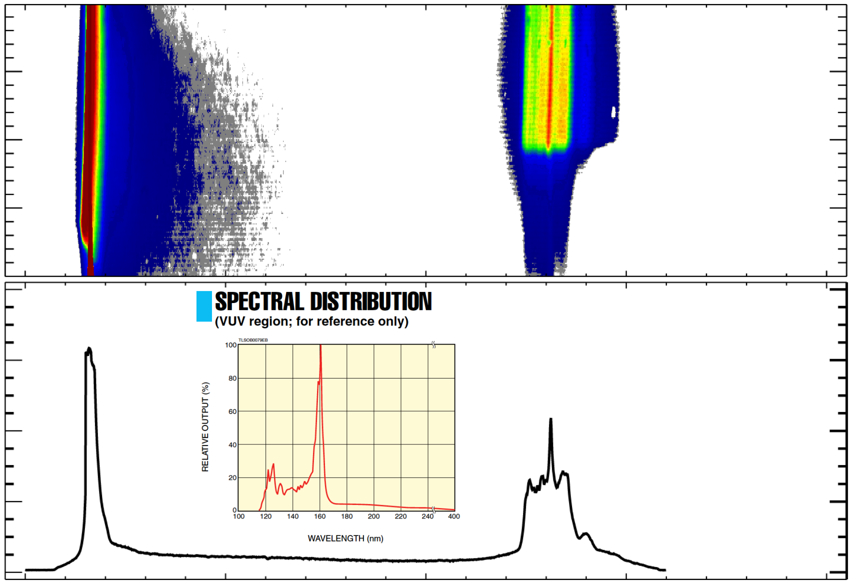

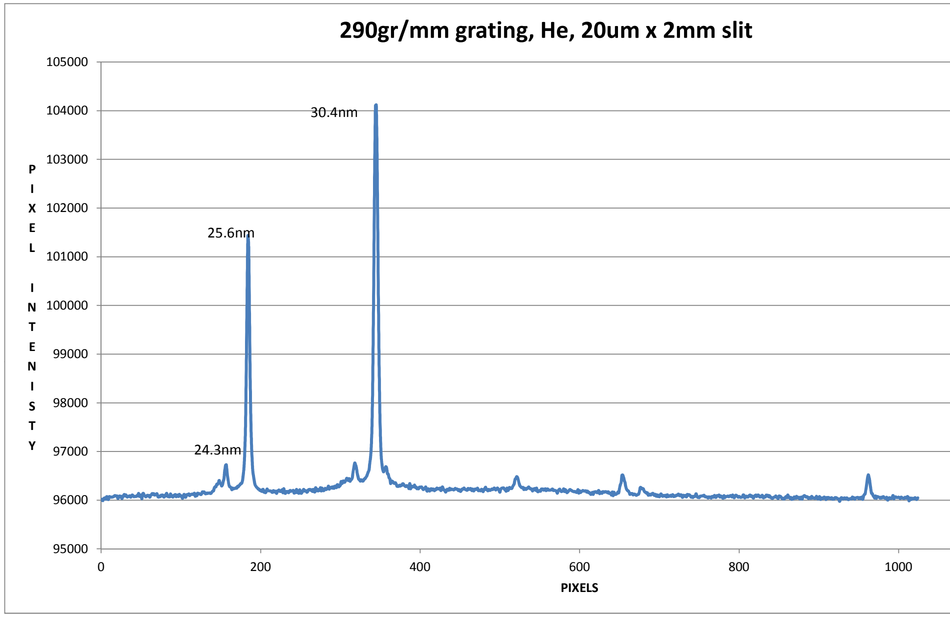

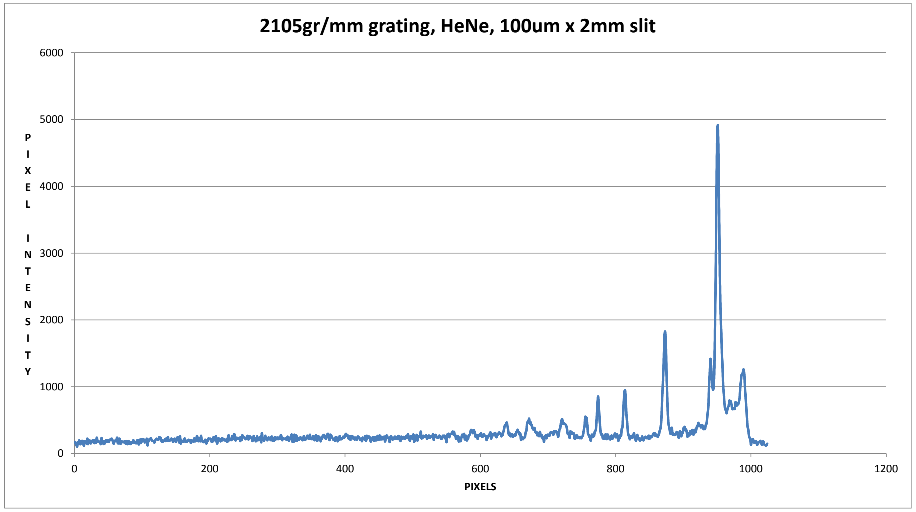

- MCP + CCD tested with Hamamatsu VUV D_2 lamp
- MCP detector tested with hollow cathode light source

VUV spectra simulations with CRETIN demonstrate feasibility of spectroscopic T_e measurements

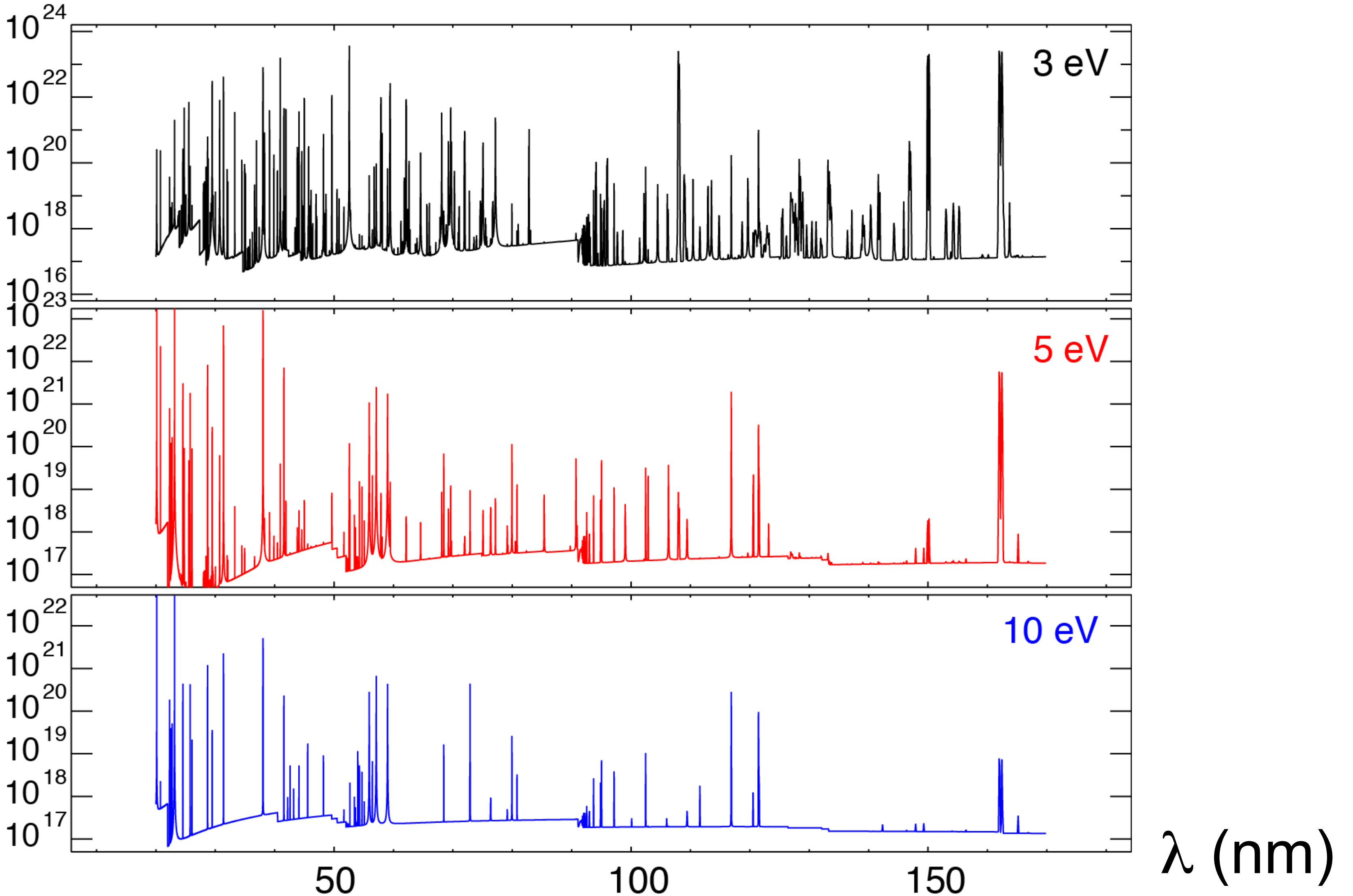

Snowflake Divertor Configuration as a Tokamak Divertor Power Exhaust Concept

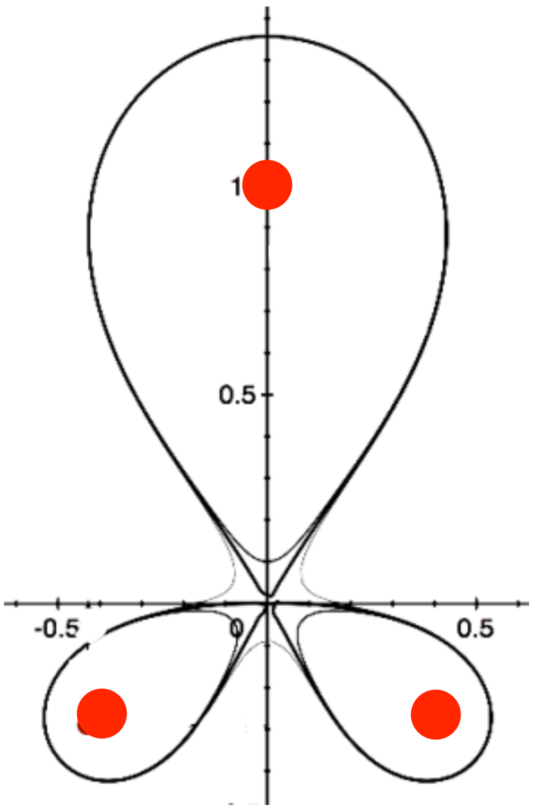

D. D. Ryutov, PoP 14, 064502 2007; PPCF 54, 124050 (2012)

- **Snowflake, 2nd order null**
  - $B_p \sim 0$, $grad\ B_p \sim 0$
    (Cf. first-order null: $B_p \sim 0$)
  - $B_p(r) \sim r^2$ (Cf. first-order null: $B_p \sim r$)
  - Four divertor legs
- **Geometry benefits**
  - Higher edge magnetic shear
  - Larger plasma wetted-area A_{wet} (f_{exp})
  - Larger parallel connection length $L_{||}$
  - Larger effective divertor volume V_{div}

  To maximize geometry benefits: $d_{XX} \leq a\ (\lambda_q\ /a)^{1/3}$
- **Transport benefits**
  - High convection zone with radius D*
  - Power sharing over four strike points
  - Enhanced radial transport (larger λ_q)

  To maximize sharing: $d_{XX} \leq D^* \sim a\ (a\ \beta_{pm}\ /\ R)^{1/3}$

Snowflake divertor enables power and particle sharing over multiple strike points

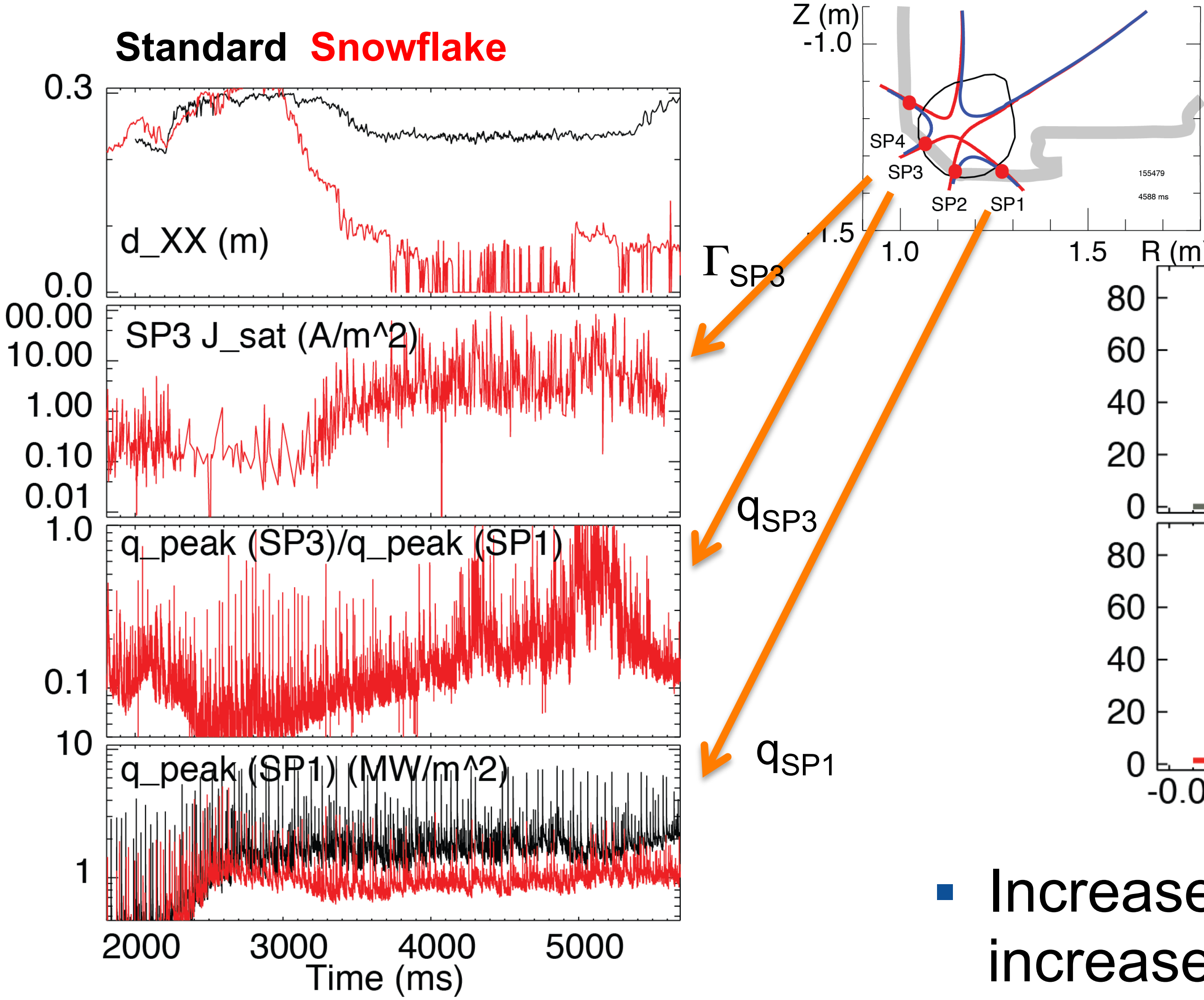

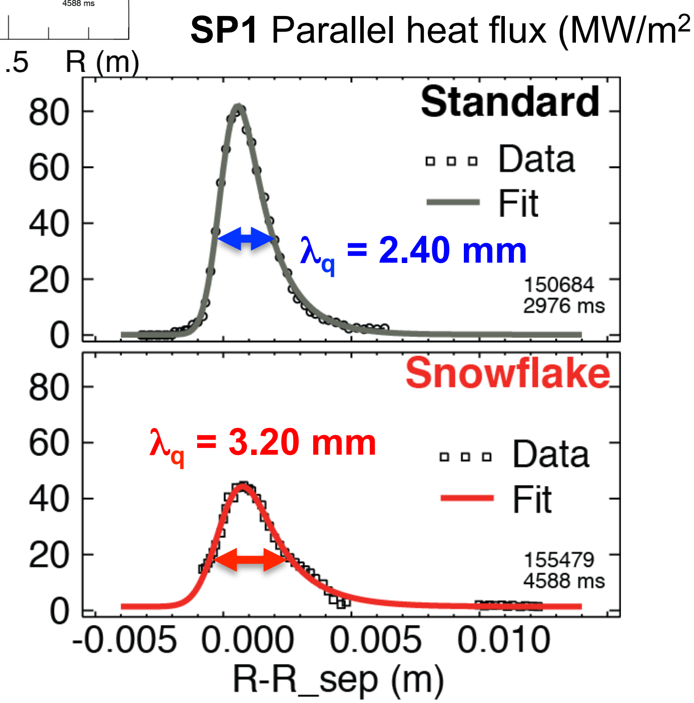

V. A. Soukhanovskii et.al, IAEA FEC 2014

- Increased λ_q may imply increased transport

- Increased λ_q may imply increased transport

Snowflake configuration favorably affects radiative divertor and detachment

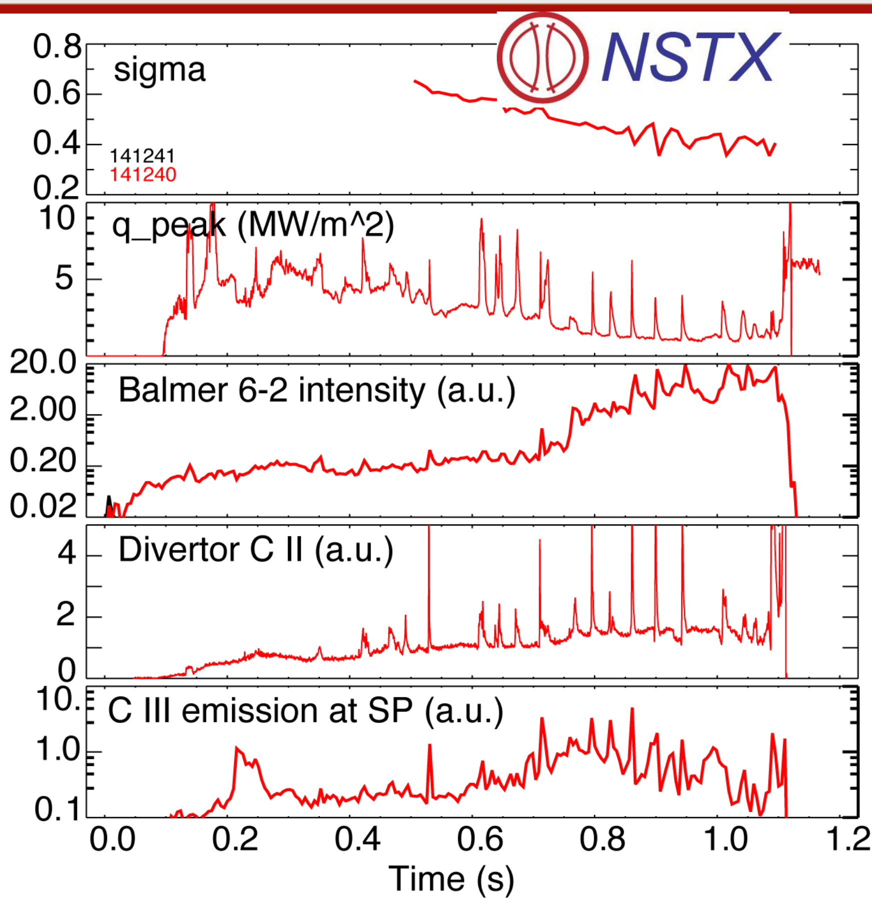

Standard **Snowflake**

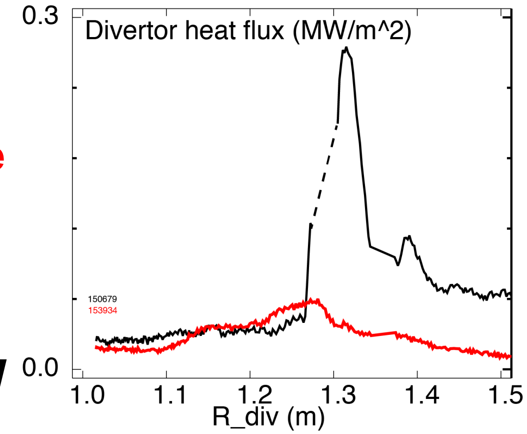

P_{SOL} = 3-4 MW

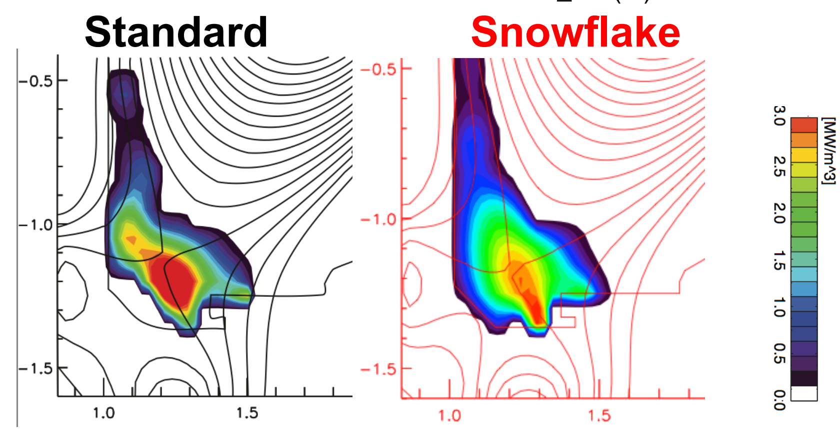

- Natural partial detachment in NSTX snowflake otherwise inaccessible with standard divertor

V. A. Soukhanovskii et.al, NF 2011; POP 2011

- Broader radiated power distribution, nearly complete power detachment in DIII-D

V. A. Soukhanovskii et.al, IAEA FEC 2014

Several important plasma effects predicted by theory in the snowflake divertor configuration

- Churning mode
  - Convective poloidal motion
  - New NSTX-U diagnostics: Doppler *v* spectroscopy and fast camera
- Divertor turbulence and blob dynamics
  - Filament splitting and shearing
  - New NSTX-U diagnostics: fast camera and fast filterscopes
- Prompt particle loss
  - D. D. Ryutov, PoP 17, 014501, 2010
  - Effect on pedestal radial electric field and ELMs
  - New NSTX-U diagnostics: Doppler T_i spectroscopy

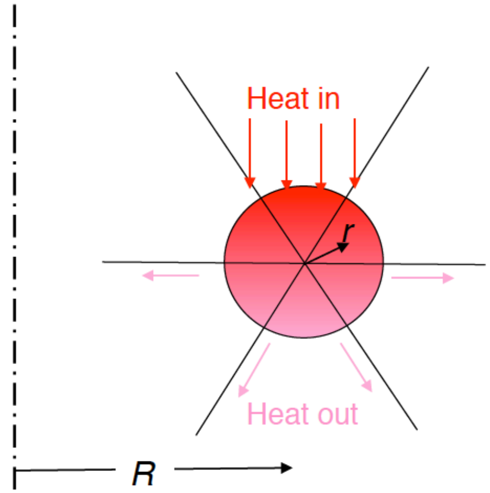

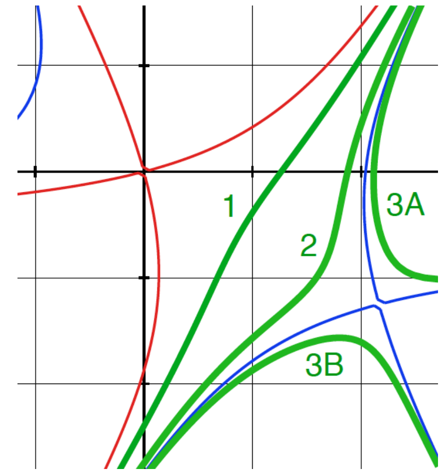

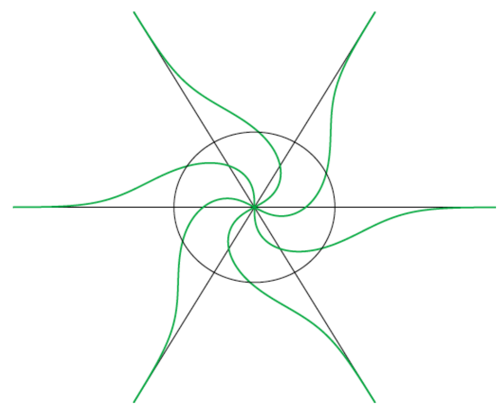

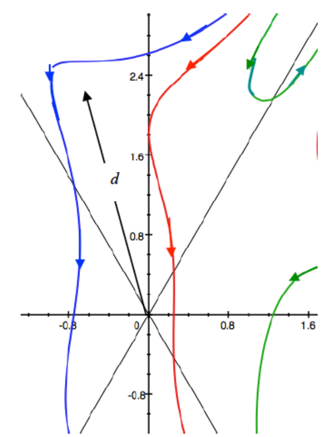

Snowflake
[affected zone: $(d/a)<(q_0\rho_i/a)^{2/5}\sim0.2$]

D. D. Ryutov, 2015 Sherwood Fusion Theory Conference

Doppler spectroscopy

- Maxwellian distribution of atom (ion) velocities lead to a Gaussian shape of projection on line of sight
- FWHM is related to temperature

$$\Delta\lambda_D = 7.16 \times 10^{-7}\lambda\sqrt{T/\mu}$$

- When ions charge-exchange with neutrals (e.g. D), neutral temperature is close to ion temperature
- Large variety of D, He, Li neutral and ion lines in UV, VIS, and NIR
- Based on PI ProEM CCD, 4 pixels 16 um each, FWHM of one instrumental line takes 64 um, or 0.064 mm
- With given McPherson 207 spectrograph imaging quality and dispersion, FWHM of Doppler broadened line must exceed 0.064 mm on the detector

High resolution divertor spectrometer will be used for divertor T_i studies

McPherson 207 with 3600 g/mm grating and Pro EM 512 CCD will have 0.027 nm instr. line

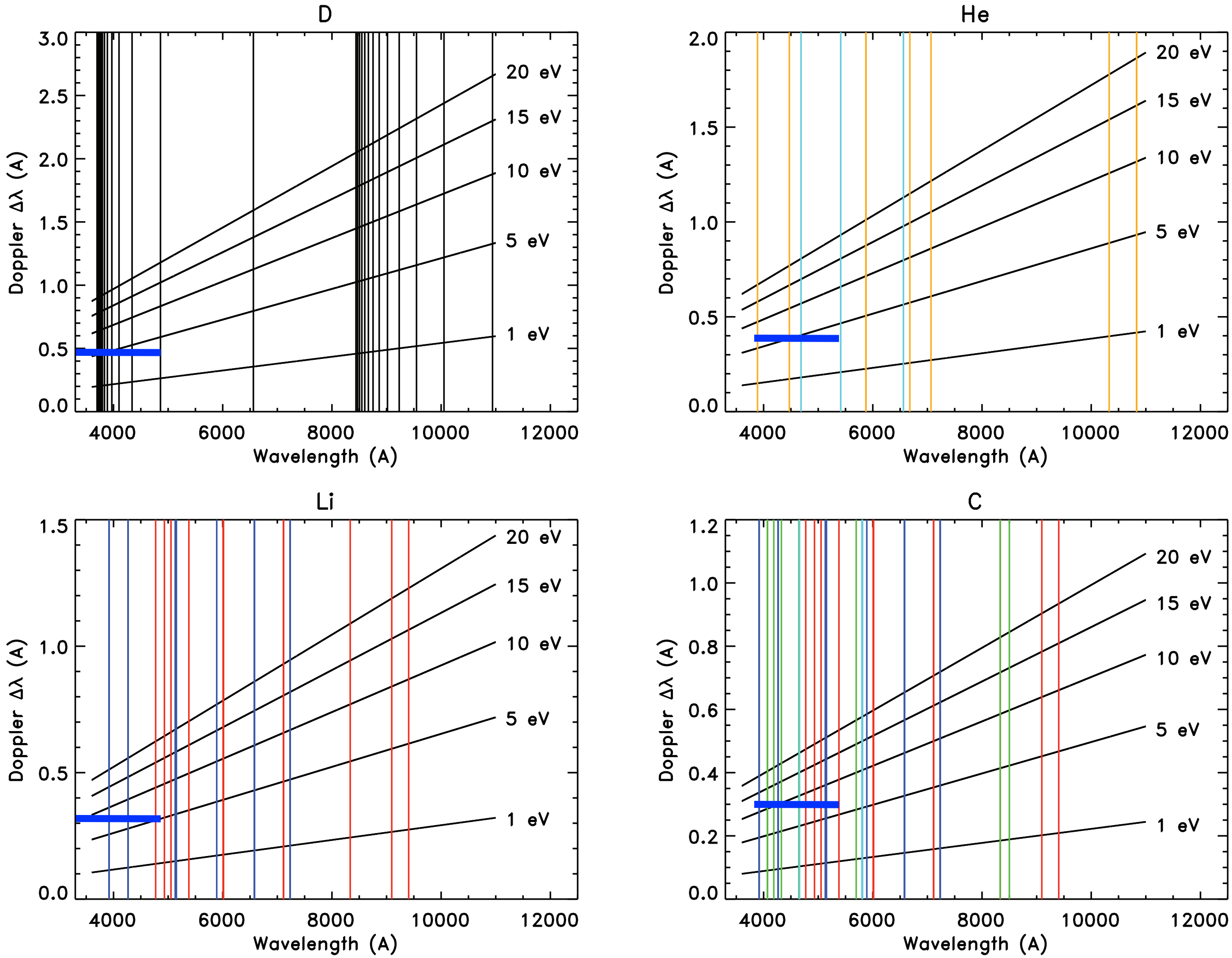

35 A on CCD chip

Fast filtered visible camera will enable divertor emission distribution and turbulence imaging

- Vision Research Phantom camera v1211
- 1280x800 pixels
- Pixel size 28x28 micron
- Chip size 35.8 x 22.4 mm

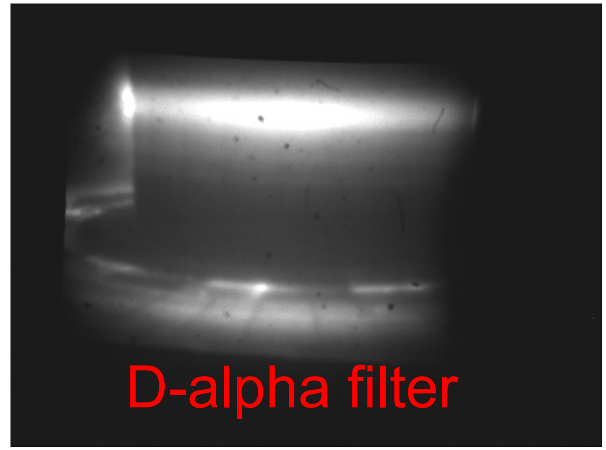

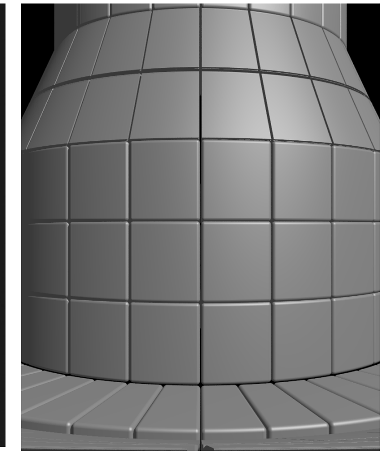

Resolution	Max kfps	Max rec time (s)
1280x800	12.6	1.3
256x256	103.4	2.42
128x128	240.3	3.85
128x64	415.1	4.06
128x32	571.0	5.0

- Planned divertor turbulence studies
  - Filament imaging
  - Turbulence metrics

New divertor diagnostics to be used for radiative divertor control development and snowflake divertor studies

- Real-time divertor T_e estimate for radiative divertor control
  - Two new spectrometers for divertor T_e
    - From UV-VIS Balmer line intensity ratios and continua intensity ratios
    - From carbon or nitrogen Li-like and Be-like ion line intensity ratios
- Churning mode, divertor turbulence and prompt particle loss studies in the snowflake divertor
  - New spectrometers for Doppler v and T_i measurements, fast cameras and fast filterscopes